Electrochemical and structural studies of nickel(II) complexes with N_2O_2 Schiff base ligands derived from 2-hydroxy-1-naphthaldehyde. Molecular structure of *N,N'*-2,3-dimethylbutane-2,3-diyl-bis(2-hydroxy-1-naphthylideneiminate) nickel(II)

M. A. A. F. de C. T. Carrondo[b,c], Baltazar de Castro[a,*], Ana Maria Coelho[b], Deolinda Domingues[a], Cristina Freire[a] and José Morais[b]

[a]*Departamento de Química, Faculdade de Ciências do Porto, 4000 Porto (Portugal)*
[b]*Centro de Tecnologia Química e Biológica, 2780 Oeiras (Portugal)*
[c]*Instituto Superior Técnico, Av. Rovisco Pais, 1000 Lisbon (Portugal)*

(Received August 23, 1992; revised October 27, 1992)

Abstract

Nickel(II) complexes with N_2O_2 Schiff base ligands based on 2-hydroxy-1-naphthaldehyde and three different diamines have been prepared and their electrochemical behaviour in $(CH_3)_2SO$ studied by cyclic voltammetry. The complexes undergo reversible one-electron oxidation in this solvent and the electrolyzed solutions show rhombic EPR spectra thus supporting metal centered oxidation to form low-spin hexacoordinate nickel(III) species with two solvent molecules coordinated axially ($g_z < g_x$, g_y; d_{z^2} ground state). The crystal structure of *N,N'*-2,3-dimethylbutane-2,3-diyl-bis(2-hydroxy-1-naphthylideneiminate) nickel(II) was determined from single crystal X-ray diffraction data collected with the use of Mo Kα radiation: space group $P2_1/n$ with $a = 7.285(8)$, $b = 26.668(17)$, $c = 11.503(7)$ Å, $\beta = 95.08(4)°$, $Z = 4$ ($R = 0.065$). The complex exhibits a novel type of packing, different from that of other nickel(II) compounds with Schiff bases, in that interaction between the monomers takes place through overlapping of the naphthyl moieties. This structure and previous X-ray structural data for the other complexes studied have provided a rationale for the $E_{1/2}$ values observed in the oxidation process.

Introduction

A theme of continued interest in inorganic chemistry is the evaluation of the effect of variation in equatorial ligand structure on the redox potential of macrocyclic complexes [1], and those of nickel complexes with macrocyclic tetraaza ligands are a case in point, since the first reports of the preparation of Ni(III) complexes of saturated tetraaza macrocyclic ligands [2]. More recently, Ni(III) complexes of tetraaza macrocyclic ligands have been used as oxidants for both inorganic and organic compounds [3, 4] and thus a knowledge of how structural modifications of the ligands will affect redox potentials of their metal complexes is of obvious importance for the design of selective reagents for oxidation or reduction. For macrocyclic tetraaza ligands a number of factors have already been identified that affect the redox potentials of their nickel complexes, that include chelate ring size, donor unsaturation, and conjugation of donor unsaturation and substituent pattern in the chelate ring [2, 5, 6]. The overall aim of the present work is to correlate the electrochemical properties of Ni(II) complexes with pseudomacrocyclic N_2O_2 Schiff base ligands derived from 2-hydroxy-1-naphthaldehyde (Scheme 1) and the stability of the respective Ni(III) complexes with electronic and steric characteristics of various ligand substituents. In particular, the molecular structure of *N,N'*-2,3-dimethylbutane-2,3-diyl-bis(2-hydroxy-1-napthylideneiminate) nickel(II) was determined and compared with the structures of other similar complexes, formed by coordination of N_2O_2 Schiff bases.

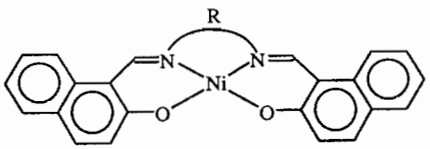

[Ni(napen)] R = $-CH_2CH_2-$
[Ni(nappd)] R = $-CH_2CH_2CH_2-$
[Ni(naptMe)] R = $-C(CH_3)_2C(CH_3)_2-$

Scheme 1.

*Author to whom correspondence should be addressed.

0020-1693/93/$6.00

© 1993 – Elsevier Sequoia. All rights reserved

Experimental

Reagents, solvents, ligands and complexes

All solvents used in the preparations were reagent grade. All reagents (nickel acetate tetrahydrate and ethylenediamine from Merck; 2-hydroxy-1-naphthaldehyde, propylenediamine and 2,3-dinitro-2,3-dimethylbutane from Aldrich) were used as received, except for ethylenediamine that was distilled prior to use. The diamine 1,1,2,2-tetramethylethylenediamine-(2,3-dimethyl-2,3-butanediamine) was prepared by a modification of the Sayre method [7].

The ligands *N,N'*-1,2-ethane-1,2-diyl-bis(2-hydroxy-1-naphthylideneimine) [H_2napen], *N,N'*-1,3-propane-1,3-diyl-(2-hydroxy-1-naphthylideneimine) [H_2nappd] and *N,N'*-2,3-dimethylbutane-2,3-diyl-bis(2-hydroxy-1-naphthylideneimine) [H_2naptMe] were prepared by standard methods [8, 9]. Typically, an ethanolic solution of the diamine was added to a rapidly stirred solution of the aldehyde and the resulting mixture was then refluxed. Yellow solids formed on cooling were collected by filtration, washed with cold ethanol and diethyl ether, and dried under vacuum.

The nickel(II) complexes *N,N'*-1,2-ethane-1,2-diyl-bis(2-hydroxy-1-naphthylideneiminate) nickel(II) [Ni(napen)], *N,N'*-1,3-propane-1,3-diyl-(2-hydroxy-1-naphthylideneiminate) nickel(II) [Ni(nappd)] and *N,N'*-2,3-dimethylbutane-2,3-diyl-bis(2-hydroxy-1-naphthylideneiminate) nickel(II) [Ni(naptMe)] were prepared by standard procedures [8, 9]; ethanolic solutions of the ligands were added to ethanolic nickel(II) acetate solutions; the mixtures were refluxed and after cooling, brown or red-brown microcrystalline solids were collected by filtration, washed with ethanol and diethyl ether, and dried under vacuum. X-ray quality crystals of [Ni(naptMe)] were obtained by slow evaporation of chloroform:acetonitrile (1:1) solutions of the complex.

[Ni(naptMe)]: ^{1}H NMR ($CDCl_3$, 200 MHz, 297 K): δ 1.43 and 1.52 (12H, $C(CH_3)_2C(CH_3)_2$), 7.13–7.76 (12H, aromatic *H*), 8.38 (2H, =C*H*). Electronic spectra: λ_{max} (nm) (ϵ (dm^3 mol^{-1} cm^{-1})): 545 (300), 445 (6750), 425 (8300), 405 (5600) ($(CH_3)_2SO$); λ_{max} (nm): 550, 460, 425, 400 (Nujol). *Anal.* Calc. for $C_{28}H_{26}N_2O_2Ni$: C, 69.9; H, 5.5; N, 5.8. Found: C, 69.6; H, 5.5; N, 5.7%.

Ni(napen)]: ^{1}H NMR ($(CD_3)_2SO$, 200 MHz, 297 K): δ 6.98–8.21 (12H, aromatic *H*), 8.90 (2H, =C*H*). Electronic spectra: λ_{max} (nm) (ϵ (dm^3 mol^{-1} cm^{-1})): 540 (300), 450 (5600), 425 (7800), 400 (5000) ($(CH_3)_2SO$); λ_{max} (nm): 540, 460, 430, 405 (Nujol). *Anal.* Calc. for $C_{24}H_{20}N_2O_2Ni$: C, 67.8; H, 4.3; N, 6.6. Found: C, 67.3; H, 4.3; N, 6.6%.

[Ni(nappd)]: ^{1}H NMR ($CDCl_3$, 200 MHz, 297 K): δ 2.04 (2H, $CH_2CH_2CH_2$), 3.66 (2H, $CH_2CH_2CH_2$), 7.15–7.76 (12H, aromatic *H*), 7.98 (2H, =C*H*). Electronic spectra: λ_{max} (nm) (ϵ (dm^3 mol^{-1} cm^{-1})): 570 (150), 440 (4600), 425 (9200), 405 (7700) ($(CH_3)_2SO$); λ_{max} (nm): 550, 445, 425, 400 (Nujol). *Anal.* Calc. for $C_{25}H_{22}N_2O_2Ni$: C, 68.4; H, 4.6; N, 6.4. Found: C, 68.6; H, 4.6; N, 6.3%.

The electrochemical measurements were performed in dimethyl sulfoxide (Merck, pro analisy); tetraethylammonium perchlorate (TEAP) was prepared by published methods [10].

Physical measurements

Elemental analysis (C, H and N) were performed at the Microanalytical Laboratory, University of Manchester. NMR spectra were recorded on a Bruker AC 200 spectrometer at 25 °C using tetramethylsilane as internal reference; electronic spectra were recorded at room temperature with a Cary 17 DX spectrophotometer.

Electrochemical measurements were made with a VA-Detector E 611, a VA-Scanner E 612 and a Coulometer E 524 (all from Metrohm) using solutions *c.* 1 mM in complex and 0.1 M TEAP. Cyclic voltammetry was performed in $(CH_3)_2SO$, with a platinum microsphere as working electrode, a platinum wire as counter electrode and an Ag/AgCl (1 M NaCl) reference electrode. In all cases, ferrocene was added at the end of the experiment and used as an internal standard. All potentials are reported relative to Ag/AgCl (1 M NaCl) reference electrode and to $E_{1/2}$ of the ferrocenium/ferrocene (Fc^+/Fc); under the experimental conditions used (scan rate 50 mV s^{-1}) the $E_{1/2}$ of the Fc^+/Fc couple is 480 mV in $(CH_3)_2SO$. The measured potentials were not corrected for junction potentials.

Coulometry was carried out at controlled potential (about 50 mV more positive than the anodic peak potential, except for [Ni(naptMe)], where the anodic peak potential was used), in a three electrode cell, using a platinum gauze electrode, a platinum foil as counter electrode and an Ag/AgCl (1 M NaCl) reference electrode (all from Metrohm).

EPR spectra were obtained with a X-band Varian E 109 spectrometer (9 GHz) equipped with a variable-temperature accessory. Spectra were calibrated with diphenylpicrylhydrazyl (dpph; $g = 2.0037$); the magnetic field was calibrated by use of Mn^{2+} in MgO. Spectra were recorded at −140 °C using sealed quartz tubes and the reported EPR parameters were obtained by computer simulation, in the usual manner [11].

Crystallography

Data collection

X-ray intensity data diffracted by a single crystal of [Ni(naptMe)] were collected on a FAST area detector diffractometer equipped with a FR571 rotating molybdenum anode generator ($\lambda = 0.71069$ Å), operating at 50 kV and 60 mA and a graphite monochromator. A

crystal to detector distance of 45 mm and a swing angle of $\theta = 26°$ were used. The exposure time was 15 s per frame with an increment of 0.25° between frames. At $\chi = 0°$, one scan of 95° through ω was done, followed by a second 95° scan with φ shifted 90° from the previous position. The missing data were then recorded by making two 90° ω scans at $\chi = 45°$, with a 90° φ shift, and two final 70° ω scans at $\chi = 90°$, again 90° apart in φ.

The initial values of the cell parameters were determined by an autoindexing procedure applied to 50 intense reflections covering two narrow (about 5° wide) and nearly orthogonal regions of reciprocal space. Throughout the data collection process, the cell parameters, based on more than 200 intense reflections, were refined together with the orientation matrix, every 10° of measured data. The values used in the structure determination and refinement are the mean and the corresponding standard deviations calculated from those refined values obtained throughout the refinement.

The data were evaluated on-line using the modified MADNES [12, 13] software for small molecules, SADNES. With this procedure, a total of 21496 reflections was measured, which reduced to 5286 unique, meaning 98% of the theoretically predicted reflections. Data reduction, including Lorentz and polarization corrections, was carried out by the Kabsch profile fitting method using program PROCOR [14]. The data were then scaled and merged with the program SHELX76 [15] giving an R_{merge} of 6.7%. Crystallographic data for the complex [Ni(naptMe)] are summarized on Table 1.

Structure determination and refinement

Systematic absences were consistent with space group $P2_1/n$ (No. 14). The position of the Ni atom was obtained from a Patterson synthesis; all the remaining atoms were found from electron density difference Fourier syntheses. Isotropic refinement of all the atoms converged to $R = 0.135$. Some cycles of anisotropic refinement for all non-hydrogen atoms yielded $R = 0.079$. Subsequent difference Fourier syntheses revealed the position of all hydrogen atoms which were inserted and allowed to refine isotropically. The large number of parameters prevented a free refinement for all of them; thus, the hydrogen positions in each CH_3 group were refined with the same thermal parameter. A weighting scheme was introduced to give the final $R = 0.065$ and $R_w = 0.071$ ($w = 1.1256/[\sigma^2(F) + 0.004964F^2]$).

The final atomic positional parameters are given in Table 2. All computations required to solve and refine the structure were made by use of SHELX76 [15], drawings were made by use of ORTEP [16]. Atomic scattering values were taken from the International Tables [17]. See 'Supplementary material'.

TABLE 1. Crystallographic and data collection parameters for the complex [Ni(naptMe)]

Crystal data	
Formula	$C_{28}H_{26}N_2O_2Ni$
Molecular weight	481.236
Space group	$P2_1/n$
a (Å)	7.285(8)
b (Å)	26.668(17)
c (Å)	11.503(7)
β (°)	95.08(4)
V (Å^3)	2226.0
Z	4
Mosaic spread	0.910
D_c (g cm^{-3})	1.436
μ(Mo Kα) (cm^{-1})	8.71
F(000)	1008
Data collection	
No. measured reflections	21496
No. unique reflections	5286
No. reflections with $F > 3.0\ \sigma(F)$	3122
No. parameters	394
Largest shift/e.s.d.	5.35
Residual electron density (e Å^{-3})	0.83
R	0.065
R_w[a]	0.071

[a] $R_w = \Sigma(|F_o - F_c|w^{1/2})/\Sigma(F_o w^{1/2})$; $w = 1.1256/[\sigma^2(F) + 0.004964F^2]$.

Results

Ni(II) complexes with the ligands napen, nappd and naptMe have been prepared and characterized by common methods: elemental analysis, NMR data, absorption electronic spectra obtained in solid mulls and in $(CH_3)_2SO$. NMR spectra of the complexes have the ligand bands shifted to higher magnetic field relative to those of the free ligands. Electronic spectra in Nujol and in $(CH_3)_2SO$ are similar, and show two main features: one broad band of low intensity ($\epsilon \approx 150$ to 300 mol^{-1} cm^{-1}) that occurs at $\lambda \approx 540/570$ nm, and that is partially superimposed on a group of several high intensity bands ($\epsilon \approx 4600$ to 8300 mol^{-1} cm^{-1}) that occur at lower wavelengths. Low intensity band maxima remain unchanged when the complexes are solubilized in $(CH_3)_2SO$, except for [Ni(nappd)] for which a bathochromic shift of 20 nm is observed for the low intensity band.

Cyclic voltammetry

Oxidation of the free ligands and of the complexes was studied by cyclic voltammetry in $(CH_3)_2SO$ in the 300–1300 mV range and the results are summarized in Table 3. Ligand anodic peaks occur at more positive potentials than those used, but the complexes show one anodic and one cathodic wave (Fig. 1). The anodic–cathodic peak potential separation is larger (100–160 mV; scan rate 50 mV s^{-1}) than expected theoretically for a one-electron reversible process [18];

TABLE 2. Atomic positional parameters ($\times 10^4$) for the complex [Ni(naptMe)]

	x	y	z
Ni	1822(1)	2292	4809(1)
O(1)	1792(6)	2146(1)	6367(3)
N(1)	2277(6)	1645(1)	4387(3)
C(11)	2969(9)	1610(2)	3201(5)
C(12)	4977(8)	1813(3)	3261(6)
C(13)	2857(10)	1071(2)	2702(5)
C(14)	2152(8)	1248(2)	5049(5)
C(30)	1638(7)	1705(2)	6841(4)
C(31)	1698(7)	1244(2)	6217(4)
C(32)	1497(6)	774(2)	6814(4)
C(33)	1445(8)	303(2)	6261(5)
C(34)	1267(8)	−133(2)	6868(5)
C(35)	1112(8)	−130(2)	8062(5)
C(36)	1122(8)	319(2)	8632(5)
C(37)	1285(6)	777(2)	8026(4)
C(38)	1288(8)	1244(2)	8616(5)
C(39)	1447(8)	1682(2)	8062(5)
O(2)	1483(5)	2948(1)	5234(3)
N(2)	1768(6)	2435(1)	3248(3)
C(21)	1734(9)	1973(2)	2483(4)
C(22)	−295(10)	1763(3)	2387(6)
C(23)	2345(11)	2082(2)	1282(5)
C(24)	1564(8)	2869(2)	2765(4)
C(40)	1404(7)	3340(2)	4566(4)
C(41)	1471(6)	3336(2)	3354(4)
C(42)	1409(7)	3799(2)	2699(4)
C(43)	1591(8)	3822(2)	1490(5)
C(44)	1495(9)	4274(2)	903(5)
C(45)	1285(9)	4716(2)	1490(5)
C(46)	1138(8)	4713(2)	2662(5)
C(47)	1212(7)	4261(2)	3294(5)
C(48)	1122(8)	4249(2)	4508(5)
C(49)	1230(8)	3818(2)	5117(5)

however, under similar conditions the peak separation for the couple Fc^+/Fc is 100 mV. With increasing scan rates a linear dependence is observed between E_p and i_p and between i_p and $v^{1/2}$. The ratio i_{pc}/i_{pa} is practically equal to 1 for the scan rates studied (10–100 mV s^{-1}); however for [Ni(naptMe)] the ratio is slightly smaller than 1.0, a fact that can be traced to errors associated with the estimation of i_p, due to the close proximity of the ligand oxidation wave. Values of $E_{1/2}$ for the oxidation process Ni(II)/Ni(III) of the systems studied show that the least positive value is observed for [Ni(nappd)], whereas the most positive value occurs for [Ni(naptMe)].

Electrolysis of the Ni(II) complexes

Electrochemical oxidation of the Ni(II) complexes in $(CH_3)_2SO$ produces a change in solution colour from reddish to dark brown, implying the formation of new species. The observation that room temperature (20 °C) EPR spectra of oxidized complex solutions in $(CH_3)_2SO$ exhibit a single broad line, with g_{iso} values

TABLE 3. Electrochemical data for Ni(II) complexes in 0.1 M TEAP in $(CH_3)_2SO$ and EPR parameters for their electrochemically oxidized solutions[a,b]

Complex	Cyclic voltammetry data						EPR parameters[c]				
	Ag/AgCl (1 M NaCl)				Fc^+/Fc	i_{pc}/i_{pa}[d]	g_x	g_y	g_z	g_{av}	g_{iso}
	E_{pa}	E_{pc}	ΔE	$E_{1/2}$	$E_{1/2}$						
[Ni(napen)]	838	718	120	778	298	1.0	2.269	2.211	2.018	2.166	2.192
[Ni(nappd)]	693	560	133	627	147	1.0	2.264	2.222	2.029	2.172	2.184
[Ni(naptMe)]	945	845	100	895	415	0.9	2.268	2.221	2.018	2.169	2.182

[a]All potentials in mV. Solute concentration $\approx 10^{-3}$M; scan rate = 50 mV/s; $\Delta E = E_{pa} - E_{pc}$; $E_{1/2} = \frac{1}{2}(E_{pa} + E_{pc})$; and E_{pa} and E_{pc} are the anodic and cathodic peak potential, respectively. Under the conditions used, $E_{1/2}$ (Fc^+/Fc) is 480 mV. [b]The nickel(III) species in solution are formulated as $[NiL((CH_3)_2SO)_2]^+$, where L is a Schiff base ligand, see text for details. [c]The value of g_{av} is $1/3(g_x + g_y + g_z)$; g_{iso} was obtained from fluid solution EPR spectra at 20 °C. [d]The ratio i_{pc}/i_{pa} is constant for scan rates in the range 20–100 mV/s.

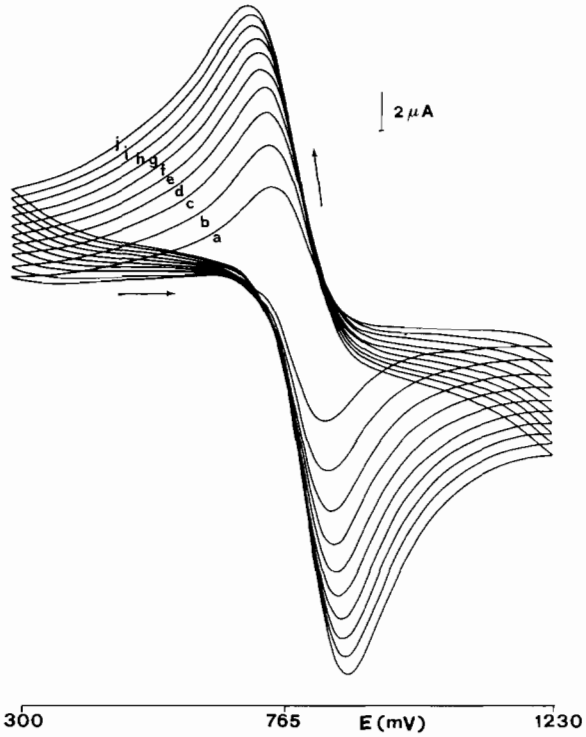

Fig. 1. Variable-scan-rate cyclic voltammograms of [Ni(napen)] in $(CH_3)_2SO$/0.1 M TEAP; peak potentials vs. Ag/AgCl (1 M NaCl) scan rate (mV/s): (a) 10, (b) 20; (c) 30; (d) 40; (e) 50; (f) 60; (g) 70; (h) 80; (i) 90; (j) 100.

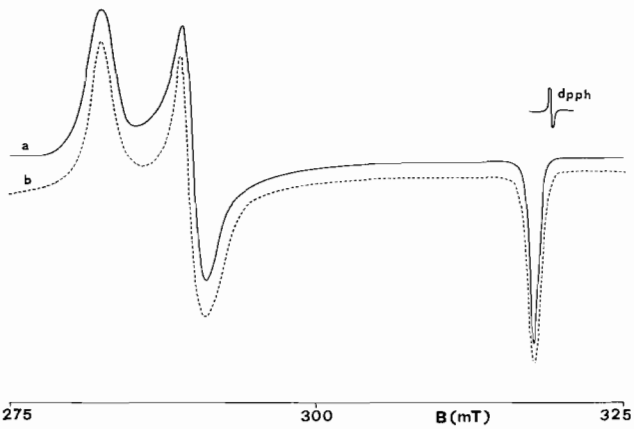

Fig. 2. Frozen solution X-band EPR spectrum at −140 °C of (a) electrochemically oxidized solution of [Ni(napen)] and (b) computer simulation of (a) using the parameters in Table 3.

of 2.192, 2.184 and 2.182 for [Ni(napen)], [Ni(nappd)] and [Ni(naptMe)], respectively, strongly suggests a metal-centered oxidation process. It must be pointed out that the EPR spectra of [Ni(naptMe)] also show a band at $g \approx 2.00$. At room temperature, EPR of the oxidized complexes decay to EPR silent species in about 2 h.

Frozen solution EPR spectra of the electrolytically generated nickel complexes (Fig. 2) show rhombic symmetry, large g tensor anisotropy and no superhyperfine splitting assignable to the equatorial nitrogen atoms. EPR spectra with large g tensor anisotropy and g_{iso} in excess relative to the g value of the free electron, suggest a metal centred unpaired electron, which for nickel must be associated with the d^7 low-spin electron configuration expected for a +3 formal metal oxidation state [19–21].

For [Ni(naptMe)] a small signal at $g \approx 2.00$ is also observed in frozen solutions. However, when electrolysis was made at a potential value 100 mV higher than the anodic peak potential, the resulting solutions exhibit for all complexes EPR spectra that show bands typical of Ni(III) species and also a small signal centered at $g \approx 2.00$. These observation suggests that ligand oxidation takes place at potentials similar to those of the complexes (*vide supra*) and that the band at $g = 2$ must be due to radical species formed by oxidation of the coordinated ligand.

In the absence of EPR crystal data for our complexes, the observed similarity between their g features and those of analogous cobalt(II) compounds [22] can be further extended to support the following orientation scheme for the tensor axes in the nickel complexes: $g_1 = g_x$, $g_2 = g_y$ and $g_3 = g_z$, where g_1 and g_3 refer to the lowest and highest magnetic field g values, respectively. The g values of the complexes are summarized in Table 3.

The observed g pattern is similar to that of g values for Ni(III) hexacoordinate complexes for which a $^2A_1$ (d_{z^2}) ground state was assumed [19–21] and, although no hyperfine splittings with coordinate solvent atoms can be observed (^{16}O has non-magnetic nuclei), the same ground state is assumed and the structure $[NiL(DMSO)_2]^+$ is proposed for these complexes, where L is napen, nappd and naptMe [21]. Furthermore, the observation that $g_z < g_x, g_y$ implies axial elongation along the z axis, leading to a $C_{2v}(x)$ molecular symmetry, as would be expected for an almost planar tetracoordenate N_2O_2 ligand.

X-ray crystal structure of [N(naptMe)]

Bond lengths and bond angles are given in Table 4, and a molecular diagram with atomic numbering scheme is represented in Fig. 3. The coordination geometry around the metal atom is square planar with the ligand naptMe coordinated through the nitrogen and oxygen atoms in a *cis* configuration of type N_2O_2. The N_2O_2 coordination square is almost planar, with a maximum deviation from planarity of −0.045(5) Å at N(1) and with the metal atom 0.002(2) Å away from that plane. Atoms C(11) and C(21) on the ethylenediamine bridge deviate −0.486(6) and 0.273(7) Å from the plane NiN_2O_2, and the torsion angle N(1)–C(11)–C(21)–N(2)

TABLE 4. Bond lengths (Å) and bond angles (°) for the complex [Ni(naptMe)]

Bond lengths							
Ni–O1	1.837(5)	Ni–O2	1.839(5)	C31–C30	1.426(7)	C41–C40	1.399(8)
Ni–N1	1.832(6)	Ni–N2	1.832(6)	C39–C30	1.426(8)	C49–C40	1.435(8)
C30–O1	1.304(7)	C40–O2	1.294(7)	C32–C31	1.443(7)	C42–C41	1.444(7)
C14–N1	1.310(7)	C24–N2	1.286(7)	C33–C32	1.408(8)	C43–C42	1.411(8)
C11–N1	1.499(7)	C21–N2	1.513(8)	C37–C32	1.416(8)	C47–C42	1.422(8)
C31–C14	1.412(8)	C41–C24	1.424(8)	C34–C33	1.368(8)	C44–C43	1.379(8)
C12–C11	1.557(11)	C22–C21	1.575(11)	C35–C34	1.387(9)	C45–C44	1.373(9)
C13–C11	1.546(9)	C23–C21	1.516(10)	C36–C35	1.364(9)	C46–C45	1.361(9)
C21–C11	1.516(10)			C37–C36	1.417(8)	C47–C46	1.407(8)
				C38–C37	1.418(8)	C48–C47	1.405(8)
				C39–C38	1.341(8)	C49–C48	1.344(8)
Bond angles							
N1–Ni–O1	94.3(3)	N2–Ni–O2	94.1(3)	C36–C37–C32	120.1(6)		
O2–Ni–O1	85.9(2)	N2–Ni–N1	85.7(3)	C38–C37–C32	118.7(5)		
C30–O1–Ni	127.5(4)	C40–O2–Ni	127.5(4)	C38–C37–C36	121.2(6)		
C11–N1–Ni	112.5(4)	C21–N2–Ni	113.5(4)	C39–C38–C37	122.3(6)		
C14–N1–Ni	125.7(5)	C24–N2–Ni	127.0(4)	C38–C39–C30	121.7(6)		
C14–N1–C11	121.7(5)	C24–N2–C21	119.0(5)				
C31–C14–N1	126.3(6)	C41–C24–N2	126.2(6)				
C12–C11–N1	109.2(6)	C22–C21–N2	107.3(6)				
C13–C11–C12	111.0(6)	C23–C21–C22	110.7(6)				
C21–C11–N1	103.0(5)	N2–C21–C11	103.0(5)	C46–C47–C42	119.7(6)		
C21–C11–C13	112.5(6)	C23–C21–C11	114.2(6)	C48–C47–C42	118.3(5)		
C31–C30–O1	123.9(5)	C41–C40–O2	125.7(5)	C48–C47–C46	122.0(6)		
C39–C30–O1	118.0(5)	C49–C40–O2	117.1(5)	C49–C48–C47	122.1(6)		
C30–C31–C14	119.6(5)	C40–C41–C24	119.1(5)	C48–C49–C40	122.2(6)		
C32–C31–C14	120.1(5)	C42–C41–C24	120.0(5)				
C39–C30–C31	118.0(5)	C49–C40–C41	117.3(5)				
C32–C31–C30	120.0(5)	C42–C41–C40	120.8(5)				
C33–C32–C31	124.0(5)	C43–C42–C41	123.5(5)				
C37–C32–C31	119.3(5)	C47–C42–C41	119.3(5)				
C37–C32–C33	116.7(5)	C47–C42–C43	117.2(5)				
C34–C33–C32	121.8(6)	C44–C43–C42	121.1(6)				
C35–C34–C33	121.4(6)	C45–C44–C43	120.8(7)				
C36–C35–C34	118.9(6)	C46–C45–C44	120.3(6)				
C37–C36–C35	121.1(6)	C47–C46–C45	120.8(6)				

is 47.5(5)°, giving an unsymmetric *gauche* conformation to that bridge.

The six-membered metallocycle Ni, O(2), N(2), C(24), C(41), C(40) is almost planar with a maximum deviation from planarity of 0.041(6) Å at C(24) while the other six-membered ring Ni, O(1), N(1), C(14), C(31), C(30), is less planar with a maximum deviation of 0.137(5) Å at C(31). These two metallocyclic rings are nearly coplanar, the angle between the two least-square planes being 6.1(1)°. Furthermore, the two rings show almost no folding through the N...O lines; the angle between line N(1)...O(1) and the plane through N(1), C(14), C(31), C(30), O(1) is 0.4(2)°; and that between line N(2)...O(2) and the plane N(2), C(24), C(41), C(40), O(2) is 0.5(2)°. Consequently, the Schiff base, except for the ethylenediamine bridge and its methyl substitutes, is nearly planar. In Table S3 (see 'Supplementary material') the parameters that define some of the more important least-squares planes in the molecule as well as deviations of atoms from these planes are listed.

Packing diagrams for [Ni(naptMe)] presented in Figs. 4 and 5 show that the molecular planes are approximately parallel to each other, but superimposed in an alternated way with intermolecular distances for Ni...Ni $(0.5+x, 0.5-y, 0.5+z)$ of 6.623(4) Å, and for Ni...Ni $(x-0.5, 0.5-y, 0.5+z)$ of 7.161(4) Å. The naphthyl groups from symmetrically related molecules are, however, partially overlapping with a mean distance between planes of 3.568(6) Å.

Discussion

Crystal and molecular structures of [Ni(nappd)] [23] and [Ni(napen)] [24] have been published and show these complexes to be square planar like the one reported in this study. These nickel(II) complexes re-

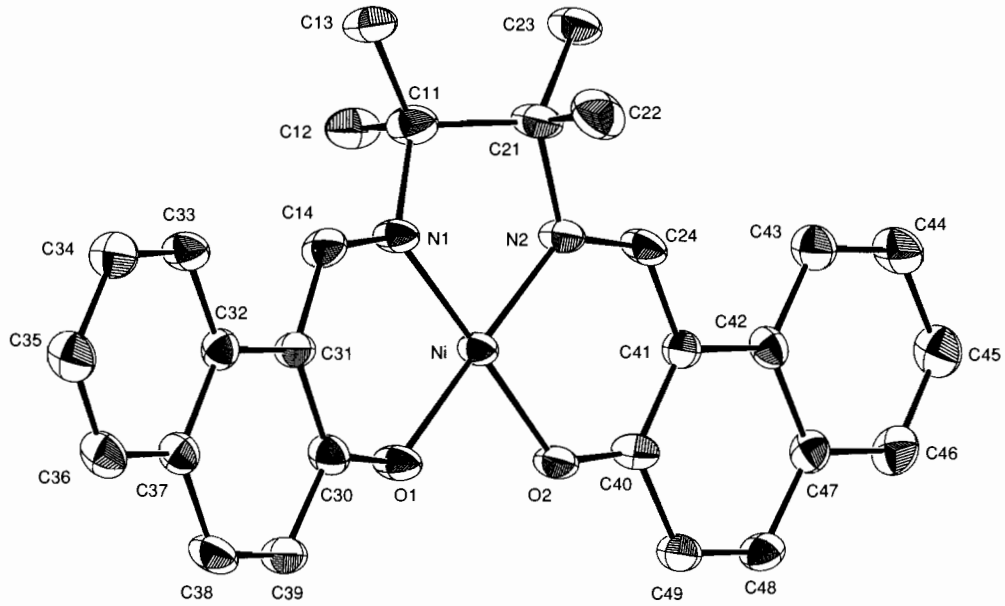

Fig. 3. ORTEP diagram of [Ni(naptMe)] showing 30% thermal ellipsoids.

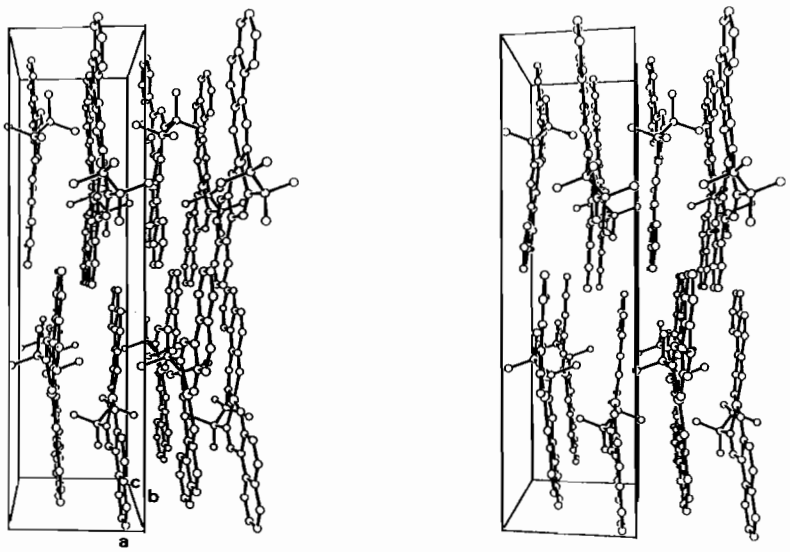

Fig. 4. Stereoscopic view of the unit cell down the *c* axis showing the quasi parallel naphthyl groups in the symmetrically related molecules.

main low spin in solution, as can be inferred from NMR and electronic data (Table 3). For [Ni(napen)] and [Ni(naptMe)], similarity between the λ values for the bands in Nujol and in $(CH_3)_2SO$, and the observed NMR chemical shifts for ligand nuclei, suggest that in this latter solvent no significant axial coordination takes place and that the complexes remain essentially square planar in solution; whereas for [Ni(nappd)], the small bathochromic shift observed in $(CH_3)_2SO$ is indicative of incipient axial coordination by solvent molecules. For [Ni(nappd)], the observed Ni–N and Ni–O distances are significantly longer than those of the other two complexes (see Table 5), thus implying a weaker equatorial ligand field. In several other nickel(II) Schiff base square planar complexes it was observed that a weak ligand field is normally accompanied by axial coordination, in solution, to strong donors; this situation must be contrasted with that observed for strong field Schiff base ligands where no axial coordination was reported.

These observations allow the assignment of the electronic transitions found in similar nickel(II) tetracoordinate low spin compounds with an N_2O_2 coordination sphere: the weaker band at 540/570 nm corresponds to transitions from the four low-lying d

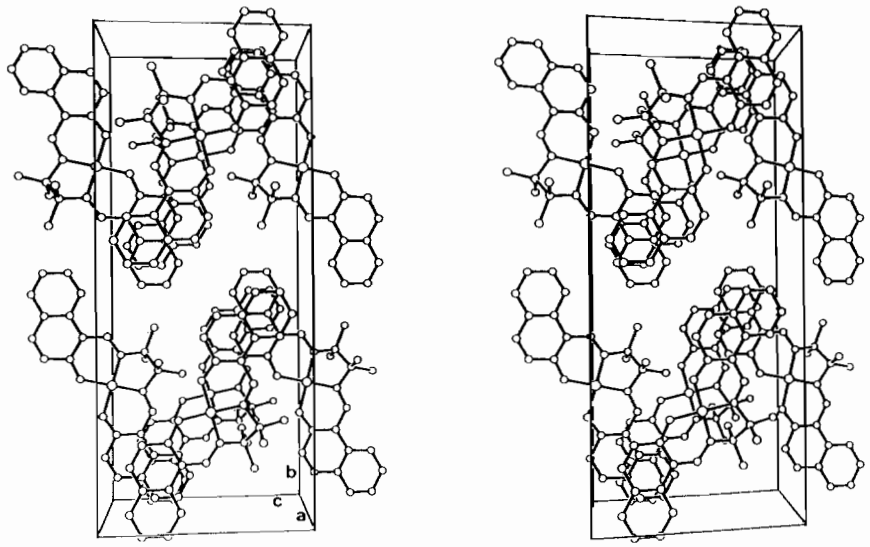

Fig. 5. Stereoscopic view of the unit cell down the *a* axis showing the overlap of the naphthyl groups.

TABLE 5. Bond lengths in the coordination sphere of the Ni atom in similar compounds

Formula	Ni–O (Å)	Ni–N (Å)	O–C (Å)	N=C (Å)	Ref.
$[Ni(C_{28}H_{26}N_2O_2)]$ Ni(naptMe)	1.837(5) 1.839(5)	1.832(6) 1.832(6)	1.304(7) 1.294(7)	1.286(7) 1.310(7)	This work
$[Ni(C_{24}H_{18}N_2O_2)]$ Ni(napen)	1.852(2) 1.847(2)	1.839(2) 1.842(2)	1.306(3) 1.312(3)	1.295(3) 1.300(3)	24
$[Ni(C_{25}H_{20}N_2O_2)]$ Ni(nappd)	1.866(6)	1.871(8)	1.285(13)	1.312(13)	23
$[Ni(C_{17}H_{16}N_2O_2)]$ Ni(salpd)	1.845(3)	1.901(4)	1.309(5)	1.303(6)	28
$[Ni(C_{16}H_{14}N_2O_2)]$ Ni(salen)	1.850(2) 1.855(2)	1.853(2) 1.843(2)	1.311(4) 1.310(4)	1.293(4) 1.301(4)	26

orbitals that have very similar energy to the empty d_{xy} orbital, as the ϵ values also support; on the other hand the very intense bands at lower wavelengths are assigned to charge-transfer transitions*.

Molecular structure of [Ni(naptMe)]

In Table 5 are presented bond distances of the coordination spheres of [Ni(naptMe)], [Ni(nappd)] [23] and [Ni(napen)] [24] and of other pseudo-macrocyclic nickel(II) complexes with an N_2O_2 coordination sphere. The average Ni–N and Ni–O bond lengths for [Ni(naptMe)], 1.832(6) and 1.838(5) Å, are the shortest reported so far. The angles centered in the metal atom have the usual values, larger than 90° when bonding six-membered chelating rings, and less than 90° when bonding five-membered rings.

*This discussion is based on a $C_{2v}(x)$ symmetry for the complex (see Scheme 1); the symmetry axes are not coincident with the Ni-coordinate bonds, and so the highest d orbital is d_{xy}.

The torsion angle N(1)–C(11)–C(21)–N(2) in [Ni(naptMe)], 47.5(5)°, is larger than the corresponding values observed in [Ni(napen)] or [Ni(salen)] [25], 34.4(2) and 34.0(3)°, respectively. This can be attributed to the bulkiness of the four methyl groups in the ethylene bridge of [Ni(naptMe)]. Two of these groups have carbon atoms approximately in the coordinating plane, whereas the other two are axial and on opposite sides of that plane (see Fig. 3).

Crystal structure of [Ni(naptMe)]

The crystal packing of [Ni(naptMe)] is completely different from that observed in other similar complexes of nickel, which normally involves dimers [24, 25] or chains of molecules [23, 26, 27] with the Ni...Ni vector nearly perpendicular to the molecular coordination planes and with Ni...Ni distances in the range 3–4 Å. For example, in [Ni(nappd)] [23] the structure is made up of parallel molecules, stacked in such a way that the Ni atoms are almost directly above each other, the

closest distance being 4.07(1) Å; whereas in [Ni(napen)][24] the molecules form centrosymmetric dimers, with the direction of the Ni...Ni bond making an angle of 76° with the $Ni(N_2O_2)$ coordination plane.

For [Ni(naptMe)] the methyl groups in the ethylene bridge are very bulky and therefore prevent these types of packing. Instead, the molecules are shifted and rotated so that the overlapping groups are now naphthyl moieties keeping, however, a reasonable parallelism between the molecular planes (Fig. 4). The nickel atoms are quite apart from each other (6.623(4) or 7.161(4) Å), but overlapping naphthyl groups are 3.568(6) Å apart, a distance comparable to the Ni...Ni distance observed in similar complexes referred to above. This is a novel crystal structure for this type of compound, where monomer–monomer interaction does not involve the nickel centers in the form of dimers or of stacks. Instead, it is asserted by overlapping of the naphthyl moieties, that stack forming chains, with π–π interactions between the monomers.

Cyclic voltammetry

In $(CH_3)_2SO$ all the complexes are oxidized to Ni(III) hexacoordinate species with two solvent molecules coordinated axially, as can be inferred from the EPR spectra of the electrolyzed solutions, in a process that closely resembles reversible charge transfer. At 50 mV s^{-1}, $\Delta E_p = 100$–130 mV (ΔE_p (Fc^+/Fc) = 100 mV) and increases slightly with the scan rate, $i_p/v^{1/2}$ is independent of the scan rate, and $i_{pc}/i_{pa} \approx 1$ [18]. These results also provide support for chemical reversibility within the cyclic voltammetry time scale.

The absolute values of $E_{1/2}$ observed for the complexes can be rationalized, taking those of [Ni(napen)] as reference and invoking solvent axial coordination in the +3 oxidation state. For [Ni(naptMe)], the high value observed for $E_{1/2}$ is opposite to the known inductive effect of the methyl groups, as an increase in the number of these groups should cause a reduction of $E_{1/2}$ due to a decrease of the electron affinity of the redox orbital [28]. However, when oxidation is accompanied by axial coordination, it has been observed that axial methyl groups may induce steric repulsions with axial ligands, thus overcoming their inductive effect and making axial coordination more difficult, causing an increase in $E_{1/2}$ values [2, 6, 29]. Such an effect has been documented for cobalt(III) complexes of salen derivatives with different numbers of methyl groups on the bridging ethylene backbone, where for one or two methyl groups the inductive effects are dominant, whereas for three or four methyls, steric effects become dominant and an anodic shift is observed for $E_{1/2}$ [6]. Also, for nickel(II) complexes with cyclam and related macrocyclic ligands, Busch and co-workers [2] have suggested that stabilization of square planar Ni(II) over hexacoordinate Ni(III) compounds for *gem*-dimethyl substitution results from steric hindrance between the axial substituents and monodentate solvent molecules that will bind to the central metal above and below the equatorial plane in the nickel(III) complexes. A similar mechanism must be operative in [Ni(naptMe)], and the high value of $E_{1/2}$ can then be traced to steric repulsions between axial methyl groups in the ethylene bridge and thc axially coordinated solvent molecules in the nickel(III) complex.

For [Ni(nappd)] the electronic and NMR data suggest that in $(CH_3)_2SO$ incipient axial coordination of solvent molecules takes place but the complex remains low-spin and, accordingly, the lower $E_{1/2}$ values for this complex can be explained by invoking the greater tendency to bind axial ligands even in the +2 oxidation, thus facilitating the oxidation process and formation of hexacoordinate Ni(III) species. For other Ni(II) complexes some form of weak axial interaction must take place with the strong donating solvent molecules to explain the coordination expansion that accompanies the oxidation process.

Coupling of electrochemical and EPR techniques have allowed for the synthesis and characterization of nickel(III) complexes in solution. On the other hand, combination of crystal and spectroscopic data for the nickel(II) complexes made it possible to rationalize the observed $E_{1/2}$ values in terms of electronic and steric characteristics of the equatorial ligands.

Supplementary material

Anisotropic thermal parameters for non-hydrogen atoms (Table S1), positional and thermal motion parameters for hydrogen atoms (Table S2), equations of least-squares planes, deviations of atoms and angle between planes (Table S3), and listing of observed and calculated structure factors for [Ni(naptMe)] may be obtained on request from the authors.

Acknowledgement

Partial financial support for this work from the Instituto Nacional de Investigação Científica (Lisboa) through contract No. 89/EXA/3 (to B.C.) is gratefully acknowledged.

References

1 K. M. Kadish, *Prog. Inorg. Chem., 34* (1986) 435.
2 F. V. Lovecchio, E. S. Gore and D. H. Busch, *J. Am. Chem. Soc., 96* (1974) 3109.

3 A. G. Lappin and A. McAuley, *Adv. Inorg. Chem., 32* (1988) 241.
4 G. van Koten, *Pure Appl. Chem., 61* (1989) 1681.
5 G. S. Patterson and R. H. Holm, *Bioinorg. Chem., 4* (1975) 257.
6 D. F. Averill and R. F. Broman, *Inorg. Chem., 17* (1978) 3389.
7 R. Sayre, *J. Am. Chem. Soc., 77* (1955) 6689.
8 R. H. Holm, G. W. Everett and A. Chakravorty, *Prog. Inorg. Chem., 7* (1966) 183.
9 S. M. Abu-El-Wafa, M. A. El-Behairy and R. M. Issa, *Bull. Soc. Chim. Fr., 3* (1987) 445.
10 S. T. Donald, Jr. and R. L. Julian, *Experimental Electrochemistry for Chemistry,* Wiley, New York, 1974.
11 J. R. Pilbrow and E. M. Winfield, *Mol. Phys., 25* (1973) 1073.
12 A. Messerschmidt and J. W. Pflugrath, *J. Appl. Crystallogr., 20* (1987) 306.
13 J. W. Pflugrath and A. Messerschmidt, *Crystallography in Molecular Biology, Meet. Abstr., Bischenberg, France, 1985.*
14 W. Kabsch, *J. Appl. Crystallogr., 21* (1988) 916.
15 G. M. Sheldrick, *SHELX*, crystallographic calculation program, University of Cambridge, UK, 1976.
16 C. K. Johnson, *ORTEP-II, Rep. ORNL-5138,* Oak Ridge National Laboratory, Oak Ridge, TN, 1976.
17 *International Tables for X-ray Crystallography,* Vol. IV, Kynoch, Birmingham, UK, 1974.
18 A. J. Bard and L. R. Faulkner, *Electrochemical Methods,* Wiley, New York, 1980.
19 A. Desideri, J. B. Raynor and C. K. Poon, *J. Chem. Soc., Dalton Trans.,* (1977) 2051.
20 J. M. Bemtgen, H. R. Gimpert and A. von Zelewsky, *Inorg. Chem., 22* (1983) 3576.
21 B. de Castro and C. Freire, *Inorg. Chem., 29* (1990) 5113.
22 C. Daul, C. W. Schlapfer and A. von Zelewsky, *Struct. Bonding (Berlin), 36* (1979) 129.
23 F. Akhtar and M. G. B. Drew, *Acta Crystallogr., Sect. B, 38* (1982) 1149.
24 F. Akhtar, *Acta Crystallogr., Sect. B, 37* (1981) 84.
25 A. G. Manfredotti and C. Guastini, *Acta Crystallogr., Sect. C, 39* (1983) 863.
26 R. P. Scaringe and D. J. Hodgson, *Inorg. Chem., 15* (1976) 1193.
27 M. G. B. Drew, R. N. Prasad and R. P. Sharma, *Acta Crystallogr., Sect. C, 41* (1985) 1755.
28 A. A. Vlcek, *Prog. Inorg. Chem., 5* (1963) 211.
29 F. Wagner and E. K. Barefield, *Inorg. Chem., 15* (1976) 408.